A Novel Multi-DOF Precision Positioning Methodology Using Two-Axis Hall-Effect Sensors

Yusuke Kawato and Won-jong Kim, *Senior Member, IEEE*

***Abstract*—A novel sensing methodology using two-axis Hall-effect sensors is proposed, where the absolute positioning of a device atop any magnet matrix is possible. This methodology has the capability of micrometer-order positioning resolution as well as unrestricted translational and rotational range in planar 3-DOF (degree-of-freedom) motions, with potential capability of measuring all 6-DOF motions. This paper presents the methodology and preliminary experimental results of 3-DOF planar motion measurements atop a Halbach magnet matrix using two sets of two-axis Hall-effect sensors. This methodology uses the Gaussian least squares differential correction (GLSDC) algorithm to estimate the relative position and orientation from the Hall-effect sensor measurements. The sensor and its algorithm are implemented to a magnetic levitation (maglev) stage positioned atop a Halbach magnet matrix. Preliminary experimental results show its position resolution capability of less than 10 μm and position accuracy of less than 1.4 mm. Controllers were designed to close the control loop for the translational motion using the GLSDC outputs at a sampling frequency of 800 Hz on a Pentek 4284 digital signal processor (DSP). Calibration was done by comparing the laser interferometers' and the Hall-effect sensors' outputs to improve the positioning accuracy. The results exhibit good repeatability.**

***Index Terms*—Hall-effect sensor, precision positioning, multi-dimensional positioner, Gaussian least squares differential correction**

I. Introduction

FOR high-precision positioning of any device such as wafer steppers, surface motors, magnetic suspension stages, or long-range scanning stages, conventional methods use laser interferometers, optical sensors, or capacitance gauges [1]–[4]. These sensors have high resolution and low positioning noise, allowing sub-nanometer position measurements. The noncontact nature of these sensors is suitable for maglev applications.

However, these sensors have downsides in cost, design, and limitations in travel range. Components of such sensors, such as mirrors, laser heads, and laser interferometers which make up the sensing system add up to be very expensive. For example, the laser interferometry setup for the maglev stage in [2] cost approximately $48,000. In terms of design, these sensors need a very good surface finish as a flat reference, where the laser beam will reflect to the laser receiver. The mirrors may become very large in order to achieve long travel range, which makes the levitated part (namely, the platen) heavy, affecting its performance and design.

Another major downside of the use of laser interferometers is the limitation in rotation. Since the laser beam reflected off the mirror must go into the laser receiver, even small rotations on the order of a few milliradians can cause the laser beam to stray off the receiver, which causes the platen to become unstable. In a practical sense, this becomes more problematic when applying large (a few millimeters) step inputs because this can cause a responsive jerk of the platen, which may cause the platen to rotate enough to cause instability.

It must also be noted that the applications of maglev devices are not only for photolithography that requires nanometer-precision positioning, but for microassembly, where nanometer resolution is not a strict requirement. Furthermore, there may be more need for larger angular displacement capabilities, which cannot be met using conventional laser interferometers.

Having these considerations, we seek for inexpensive sensors with sufficient positioning capabilities allowing large rotations, with absolute outputs with respect to position. We focus on a sensing methodology using Hall-effect sensors in this paper.

Hall-effect sensors are used in various fields, for they are contactless, small in size, reliable, low-cost, and not sensitive to harsh and polluted environmental conditions. However, they are limited in accuracy due to offset, noise, temperature, and aging effects [5]. Nevertheless, Hall-effect sensors have been utilized in various measurement techniques, such as current sensing [6], sensing the movement of ferrous metal targets with Hall-effect proximity sensors, and measuring positions of rotating machinery [7]. Previous work showed their capability in sensing rotations of less than one degree [8].

In this paper, we propose a novel methodology for 6-DOF positioning atop a magnet matrix, using multi-axis Hall-effect sensors. First, we explain the sensing mechanism and the position-calculation methodology. We demonstrate our concept by using two sets of two-axis Hall-effect sensors

Manuscript received September 14, 2004. This work was supported in part by the Texas Advanced Technology Program under Grant No.000512-0225-2001.

Y. Kawato is with Department of Mechanical Engineering, Texas A&M University, College Station, TX 77843, USA (corresponding author to provide phone: 979-845-2224; fax: 979-862-3989; e-mail: ykawato@tamu.edu).

W.-J. Kim is with Department of Mechanical Engineering, Texas A&M University, College Station, TX 77843, USA (e-mail: wjkim@tamu.edu).

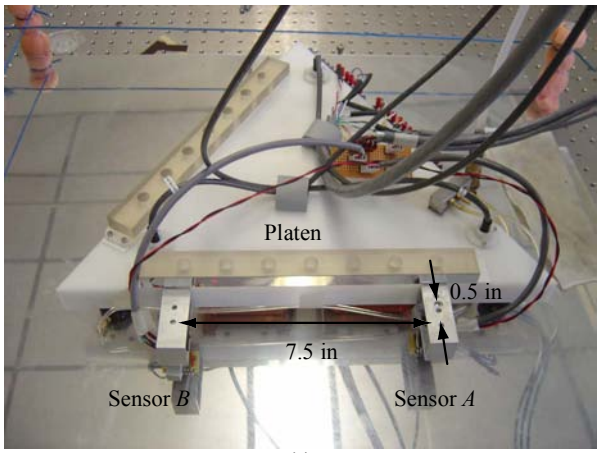

(a)

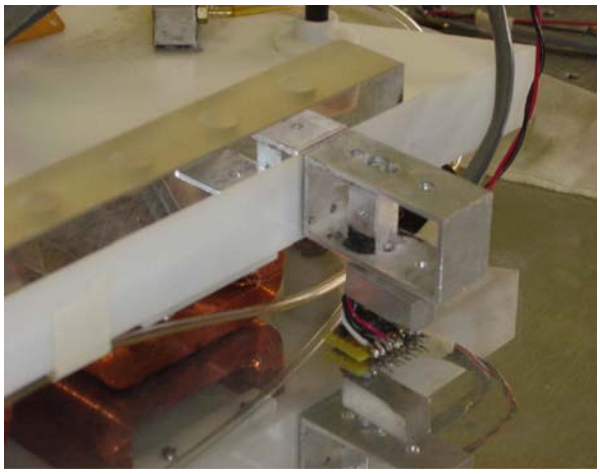

(b)

Fig. 1. Photograph of the experimental setup. (a) Multi-DOF positioner [2] with two sets of 2D-VH-11SO Hall-effect sensors mounted on the base. The triangular platen is placed atop a mirror-finished aluminum plate, and beneath the plate is the Halbach magnet matrix. (b) Close-up view of the mounted Hall-effect sensor *A*.

(Model 2D-VH-11SO by Sentron AG [9]) for 3-DOF positioning in a plane. Preliminary experimental results are presented. Our approach has many attractive features including (1) very small sensor with unrestricted range in planar (X,Y) and yaw (θ_z) motion, (2) no costly laser-interferometer setup required (a two-axis Hall-effect sensor is $10 apiece), (3) relatively simple electronic circuits with no demanding design constraints, (4) can be applied in various fields, not limited to magnetic fields, and (5) capable of sensing large rotations with sub-degree resolution.

II. Two-Axis Hall-Effect Sensing Mechanism

The methodology proposed in this paper is applicable for the positioning of a platen atop various magnetic matrices, such as [10]–[13]. In this paper, we consider positioning of a platen on a double-axis Halbach magnet matrix, presented in [2]. The platen is a magnetically levitated positioner, and is capable of positioning in 6 DOFs with 20-nm positioning resolution. The platen is currently suspended using

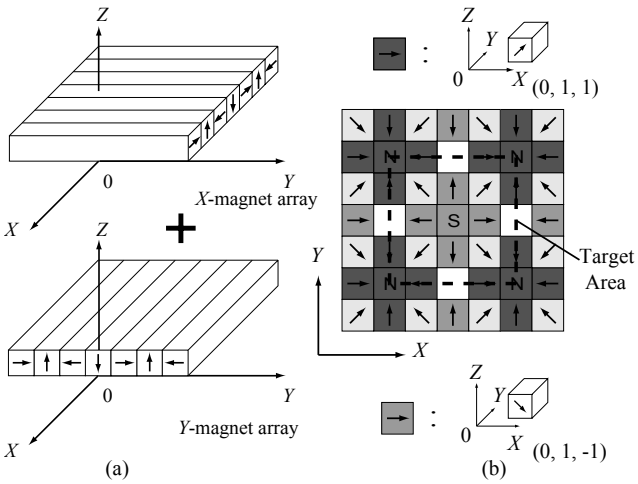

Fig. 2. Halbach magnet matrix [1], [13]. (a) Conceptual superimposition of the two orthogonal Halbach magnet arrays to produce a concentrated-field magnet matrix. (b) Top view of the concentrated-field magnet matrix

aerostatic bearings, and generates force to move in all 6 DOFs using three planar motors, which are attached to the bottom of the platen. Figure 1 (a) shows the platen with two sets of two-axis Hall-effect sensors mounted. The sensor fixture is designed such that vertical and rotational adjustments can be made. Underneath the platen is the Halbach magnet matrix covered with a mirror-finished thin aluminum plate. A close-up view of the sensor and the fixture is shown in Figure 1 (b).

A. Halbach Magnet Matrix Analysis

A conceptual construction of the Halbach magnet matrix is shown in Figure 2. The magnet matrix is a superposition of two orthogonal Halbach magnet arrays with orthogonal magnetic fields. Halbach arrays have a stronger fundamental field by a factor of $\sqrt{2}$, which allows a design of a higher power-efficient magnetic device [14].

The magnet matrix consists of two kinds of magnets. One is a strong magnet with 90° magnetization (shown with 'N' or 'S' in Figure 2), where we chose NdFeB50 material which has a remanence of $B_{r\text{strong}}$ =1.43 T. The other magnet used is a weak magnet with magnetization in 45° (shown with arrows). NdFeB30 with a remanence of $B_{r\text{weak}}$ =1.10 T was chosen, which was the weakest NdFeB at the time of purchase. The blank areas are non-magnetic aluminum spacers. The pitch of each magnet array is 50.8 mm (2"), and the dimension of each magnet and spacer is 12.7 mm × 12.7 mm × 12.7 mm (0.5" × 0.5" × 0.5"). The letters *X*, *Y*, and *Z* are used for the axes of the magnet matrix, and *x*, *y*, and *z,* the body-fixed axes of the platen.

Due to the periodicity of the magnet matrix, the magnetic flux density *B* is modeled using Fourier series. The results for B_X are shown in Figure 3. The results for an ideal Halbach array and the fabricated array are presented. The difference results from using weak magnets which differ from the ideal case,

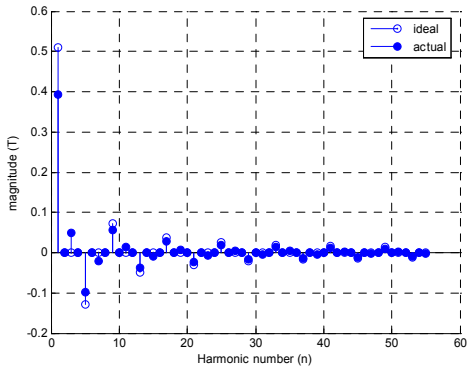

Fig. 3. Fourier coefficients of magnetic flux density B_X at 0-mm air gap

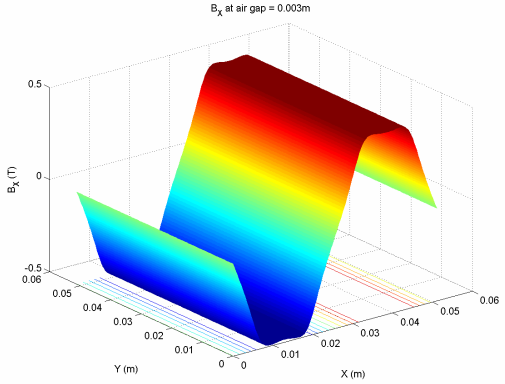

Fig. 4. Analytical result of magnetic flux density B_X of an ideal Halbach magnet matrix at 3-mm air gap

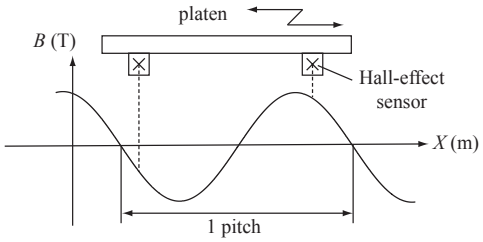

Fig. 5. 1-D positioning method

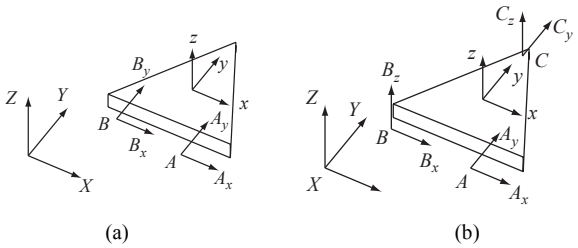

Fig. 6. Representative Hall-sensor setups with minimum number of sensor, (a) for 3-DOF position sensing in a plane, (b) for 6-DOF position sensing

$$B_{r\text{weak}} = 1.10 \neq \frac{B_{r\text{strong}}}{\sqrt{2}} = 1.01 \quad (1)$$

From this analysis, we find that for an ideal Halbach magnet matrix, the fundamental, 5th, 9th, … harmonics are non-zero and the other odd harmonics are zero. For the actual case, the fundamental and the 5th-order harmonics have the largest magnitude, and hence we chose these two harmonics as the basis functions. The curve-fitting model of the magnetic flux density at $(X_i,\ Y_i,\ Z_0)$ is in the form,

$$\begin{aligned} B_X(X_i,Y_i,Z_0) &= c+\alpha\sin(\omega X_i)+\beta\sin(5\omega X_i) \\ &\quad +\gamma\sin(\omega Y_i)+\delta\sin(5\omega Y_i), \\ B_Y(X_i,Y_i,Z_0) &= c+\alpha\sin(\omega Y_i)+\beta\sin(5\omega Y_i) \\ &\quad +\gamma\sin(\omega X_i)+\delta\sin(5\omega X_i), \end{aligned} \quad (2)$$

where $c,\ \alpha,\beta,\gamma$, and δ are the parameters to be curve-fitted. The coefficients γ and δ are included to compensate the sensor misalignment, and c is the DC offset. The curve-fitting procedure is presented in Section III.

The X-component of the total magnetic flux density in the target area is shown in Figure 4. The Y-component is identical, but the axes are reversed.

B. Proposed Sensing Method

We propose a novel methodology for a 6-DOF positioning of a platen atop a magnet matrix, using multi-axis Hall-effect sensors. This methodology will allow positioning of the platen within the 'target area' in Figure 2, which is one pitch by one pitch (50.8 mm × 50.8 mm, 2" × 2").

First, consider a case for positioning within one pitch in 1-D, as shown in Figure 5. The platen will move along the X-axis where there is a periodic magnetic field B that can be modeled as a periodic function. On the platen are two Hall-effect sensors which can detect the magnetic flux density at two points along the X-axis.

If there are two Hall-effect sensors positioned with some phase lag with respect to the pitch, it is possible to detect the unique position of the platen within one pitch, as well as the direction of motion. Further, if the Hall-effect sensors are located

$$\left(\frac{1}{4}+\frac{1}{2}n\right)\times\text{pitch},\quad n=1,2,3,... \quad (3)$$

apart, at least one sensor will be located in a 'sensitive' region where the gradient of B is large. This will allow positioning within the 'target area' to be sensitive at all locations.

Next, consider positioning in a 2-D XY plane without rotation. If there are orthogonal magnetic fields in a plane and two measurements can be taken for each axis, we can position the platen. This is precisely the reason we consider the use of magnet matrices. An example of a sensor setup for 2-D planar positioning is shown in Figure 6 (a). Note that this has only the minimum number of sensors, and having more redundant sensors will improve the resolution and accuracy of positioning.

Further, the fact that the fields B_X and B_Y are orthogonal brings one more advantage. By having four sensor outputs and two orthogonal magnetic fields, it is possible to detect

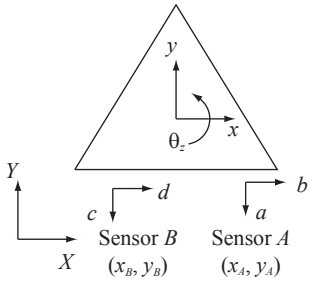

Fig. 7. Definition of sensor locations and axes of measurement

the orientation θ_z of the platen as well. This approach can be extended to 6-DOF position sensing, where in that case, the coefficients of the curve-fitting (c, α, β, γ and δ) will be modeled as a function of the air gap Z_0. One possible setup for 6-DOF position sensing is shown in Figure 6 (b).

An important part of this research is to find a way to map the nonlinear relationship between the four sensors' outputs to the position and orientation of the platen. Candidate methods for this nonlinear mapping include neural networks [15] and the GLSDC [16]. The GLSDC algorithm was implemented due to its more deterministic nature, and resulted in better convergence. Also, the GLSDC incorporates the continuous, periodic model, and the output will be continuous even when the platen goes beyond the target area.

C. Experimental Setup

A photograph of the experimental setup for 3-DOF positioning is shown in Figure 1. The platen's axes are defined at the platen's center of mass, and are not aligned with the magnet matrix's axes. The axes of measurement are shown in Figure 7. The location of the two sensors $A(x_A, y_A)$ and $B(x_B, y_B)$ are known in the body-fixed *xyz* coordinates.

A Pentek 4284 DSP is used for real-time control, and a Pentek 6102 analog-to-digital (A/D) converter board and a Datel DVME622 digital-to-analog (D/A) converter board is used for data acquisition and control. The 2D-VH-11SO Hall-effect sensor requires a 2-mA current source, which is provided using Vishay's current regulator diode CR200. The four outputs of the Hall-effect sensors are amplified by 21 times using operational amplifier circuits, and then go through an anti-aliasing filter with a corner frequency of 200 Hz. The standard deviation of the sensor output noise after filtering is about 1 mV. In Figure 7, the notation *a*, *b*, *c*, and *d* are used for the sensor's outputs after amplification and filtering, which correspond to the input channels of the Pentek 6102. The GLSDC algorithm is implemented in real-time C codes, and the routine is executed every 1.25 ms (at 800-Hz sampling frequency).

III. Sensing Algorithm

The objective of this section is to show how to resolve the position of the platen $\{X_0 \;\; Y_0 \;\; \theta_z\}^T$ from the sensor outputs $\{\tilde{a} \;\; \tilde{b} \;\; \tilde{c} \;\; \tilde{d}\}^T$ using the GLSDC algorithm. The tilde represents measured values.

A. Batch Least Squares

The GLSDC minimizes the error between the measured output and the model, and by doing so estimates the position of the platen. Hence, we must derive an appropriate model of the magnetic field for each sensor output first. The model is obtained using a method of batch least squares prior to the experiment. Consider the case for output *a* as shown in Figure 8. First, we obtain measurements as shown in Figure 8 (a). Using the method of batch least squares, we solve for the curve-fitted model shown in Figure 8 (b). The difference between the measured and modeled values is shown in Figure 8 (c). The error is found to be less than 200 mV. Possible reasons for this error are (1) fabrication error of the Halbach magnet matrix, (2) error in material properties of the magnets, (3) modeling error of the magnet matrix using batch least squares curve-fitting, (4) Hall-effect sensor misalignment with respect to the platen's axes, in θ_x, θ_y, and θ_z, (5) error in defining the precise location of the sensor (the sensitive volume of the Hall-effect sensor is 250 μm × 250 μm × 200 μm), and (6) external magnetic field interference and sensor noise. Large modeling errors may lead the GLSDC to converge to inaccurate positions, and precise adjustments in alignment must be made along with a low-noise circuit. Having such a model for each sensor

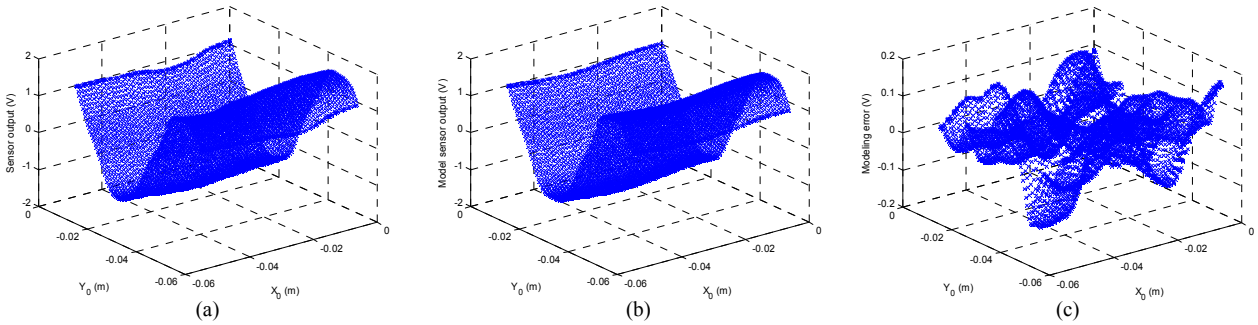

Fig. 8. Batch least squares results. (a) Sensor output *a*. (b) Curve-fitted model for output *a*. (c) Modeling error from curve-fitting

output, we proceed to the GLSDC algorithm.

B. Gaussian Least Squares Differential Correction

The GLSDC solves the nonlinear relation between the position of the platen and the sensors' outputs. A flowchart of the GLSDC algorithm is shown in Figure 9. At each time step, the input signals $\tilde{\mathbf{y}} = \{\tilde{a}\ \tilde{b}\ \tilde{c}\ \tilde{d}\}^T$ are obtained, the Jacobian matrix H is solved, and the GLSDC algorithm is executed to minimize J, the sum square of the residual errors. J decreases when the GLSDC converges, and hence an additional loop is added to check for convergence. This is a modified algorithm of the conventional algorithm presented in [16], where α is a scaling factor which is adjusted to minimize the GLSDC output's oscillation. For our experimental setup, the sensor noise's standard deviation is 1 mV, and selecting $\alpha = 0.2$ resulted in the best convergence. The GLSDC algorithm takes approximately 3 steps (3.75 ms) to converge when given a step input.

IV. Experimental Results

Experiments were conducted to test the performance of the proposed sensing method. To compare the laser interferometer and our method, the translational X and Y motions are closed using Hall-effect sensor outputs and the GLSDC algorithm, and θ_z motion is closed using the laser interferometers. This is because when the θ_z motion is closed using our method, the oscillation becomes large that the laser interferometers go out of range. This is due to the reasons mentioned in section III and can be improved by having redundant sensors.

Figure 10 shows the experimental result of a zigzag motion. A reference trajectory input to the controller is identical to Figure 10 (a), and the platen has been controlled to follow the preplanned path very well. However, the actual path of the platen detected by the laser interferometers' outputs is shown in Figure 10 (b). There is a significant deviation between the measurements from the laser interferometers and the output of the GLSDC based on the Hall-effect sensors' outputs. The maximum positioning error can be as large as 1.4 mm, as shown in Figure 10 (c). Sensor calibration and using redundant sensors may reduce this error. Because the outputs of the GLSDC are absolute and repeatable, calibration can be done by error-mapping the results of Figure 10 (c). The tabulated error is compensated using linear interpolation with the laser interferometer output as the 'true' measurements. The laser interferometer outputs are shown in Figure 11 for the two cases to a 4-mm step input. The non-calibrated result shows that the platen actually moved 4.3 mm whereas the calibrated results show that it moved 4 mm, hence following the command correctly.

The GLSDC output for 10-μm steps is shown in Figure 12. The Hall-effect sensors are capable of detecting the change

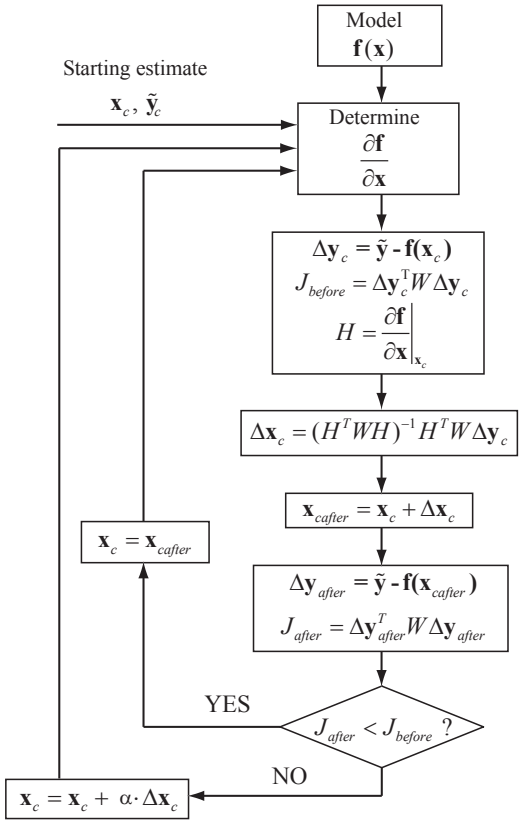

Fig. 9. Modified GLSDC algorithm [16]

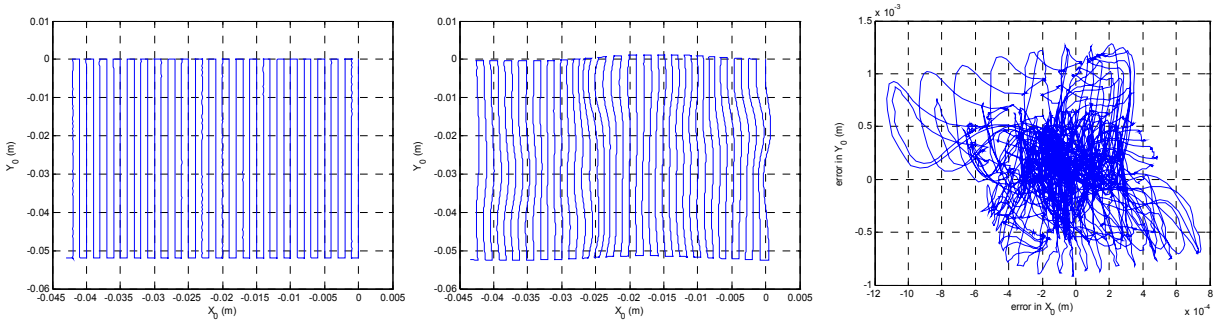

(a) (b) (c)

Fig. 10. Experimental results of positioning the platen in X and Y using the proposed algorithm. (a) Measured position from the Hall-effect sensors. (b) Measured position from the laser interferometers used for Hall-effect-sensor calibration purpose. (c) Error between the two measured values.

in magnetic flux density for position changes of less than 10 μm, and hence this method has at least 10-μm position resolution.

V. Conclusions and Future Work

We developed a novel sensing mechanism using two-axis Hall-effect sensors that have the capability to detect the position with micrometer resolution above any type of magnet matrix. The sensing mechanism and experimental results are presented in this paper. A GLSDC algorithm was implemented in real-time C codes at a sampling frequency of 800 Hz.

This sensing mechanism can also be used as a backup purpose when the sensing signal using laser interferometers becomes undetectable due to large rotation. Using two two-axis Hall-effect sensors are sufficient to estimate the position and orientation. However, there was a significant error in positioning which resulted from the reasons listed in Section III. Calibration has improved the accuracy significantly.

Currently, the translational motions in X and Y are closed using the Hall-effect sensors, and θ_z is closed using laser interferometers so that we can compare the Hall-effect sensor's performance with the laser interferometers'. Closing the remaining θ_z using this sensing method is our future work. Further, we plan to test the GLSDC algorithm with redundant sensors, which will improve the accuracy further.

Acknowledgments

The authors would like to thank Tiejun Hu, Nikhil Bhat, and Jie Gu, former graduate students of Won-jong Kim, for their contributions in this project.

References

[1] W.-J. Kim, "High-precision planar magnetic levitation." Ph.D. dissertation, Massachusetts Institute of Technology, June 1997

[2] W.-J. Kim, N. Bhat, and T. Hu, "Integrated multidimensional positioner for precision manufacturing," *Journal of Engineering Manufacture*, vol. 218, no. 4, pp. 431–442, Apr. 2004.

[3] X. Shan, S.-K. Kuo, J. Zhang, and C.-H. Menq, "Ultra precision motion control of a multiple degrees of freedom magnetic suspension stage," *IEEE/ASME Transactions on Mechatronics*, vol. 7, no. 1, pp. 67–78, Mar. 2002.

[4] M. Holmes, R. Hocken, and D. Trumper, "The long-range scanning stage: a novel platform for scanned-probe microscopy," *Precision Engineering*, vol. 24, no. 3, pp. 191–209, July 2004.

[5] C. Schott, R. Racz, F. Betschart, and R. S. Popovic, "A new two-axis magnetic position sensor," *Sensors, 2002 Proceedings of IEEE*, vol. 2, pp. 911–915, June 2002.

[6] L. Law, "Measuring current with IMC Hall effect technology," *Sensors*, vol. 3, no. 11, pp. 29–32, Nov. 2003.

[7] P. Driljace, M. Demierre, C. Schott, and R. S. Popovic, "Nonlinear effects in magnetic angular position sensor with integrated flux concentrator," *Proc. 23rd International Conference on Microelectronics*, vol. 1, pp. 223–226, May 2002.

[8] J. Trontelj, Jr,. "Functionality test for magnetic angular positioning integrated circuit," *Informacije MIDEM*, vol. 31, no. 4, pp. 287–289, 2001.

[9] Sentron AG website. [Online]. Available: http://www.sentron.ch.

[10] T. Asakawa, "Two dimensional precise positioning devices for use in a semiconductor apparatus," U.S. Patent 4 535 278, Aug. 13, 1995.

[11] W. Hinds, "Single plane orthogonally movable drive system," U.S. Patent 4 654 571, Mar. 31, 1987.

[12] D. Ebihara and M. Watada, "Study of a basic structure of surface actuator," *IEEE Transactions on Magnetics*, vol. 25, no. 5, pp. 3916–3918, Sep. 1989.

[13] D. Trumper, W.-J. Kim, and M. E. Williams, "Magnetic arrays," U.S. Patent 5 631 618, May 20, 1997.

[14] K. Halbach, "Design of permanent multipole magnets with oriented rare earth cobalt material," *Nucl. Instrum. Methods*, vol. 169, no. 1, pp. 1–10, Feb. 1980.

[15] Y. H. Hu and J.-H. Hwang, *Handbook of Neural Network Signal Processing*, 1st ed. Boca Raton, FL: CRC Press, 2002.

[16] J. L. Crassidis and J. L. Junkins, *Optimal Estimation of Dynamic Systems*, 2nd ed. Boca Raton, FL: Chapman & Hall / CRC Press, 2004.

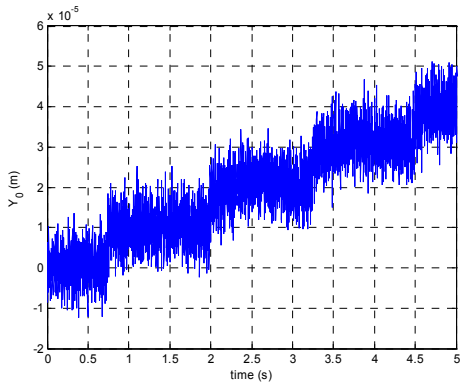

Fig. 12. Output of the GLSDC when 10-μm steps are applied to the platen

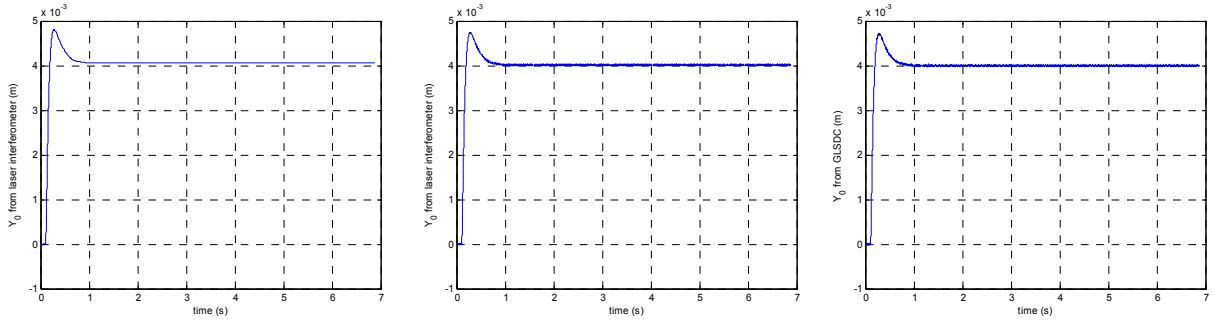

(a) (b) (c)

Fig. 11. Laser interferometer output to a 4-mm step, (a) without calibration, (b) with calibration, and (c) GLSDC output with calibration